

Modelling of heat generation in linear friction welding using a small strain finite element method

Jedrasiak P.^{a,b}, Shercliff H.R.^{a,*}

^a Department of Engineering, University of Cambridge, Trumpington St, CB2 1PZ, UK.

^b TWI, Granta Park, Cambridge, CB21 6AL, UK

* Corresponding author: hurs@eng.cam.ac.uk (44-1223-332683)

Keywords

Linear friction welding, titanium alloys, process modelling, finite element analysis.

Abstract

Heat generation in linear friction welding of Ti alloy was modelled with a computationally efficient finite element analysis. This was achieved by using multiple small strain analyses during one quarter cycle of workpiece oscillation, giving a snapshot of the average heat dissipation rate in a single complete cycle. This mechanical model for heat generation in a single cycle was then repeated at intervals throughout the equilibrium phase of welding. A separate continuous thermal model of the process [1], provided the spatial temperature field as an input to each mechanical analysis. The values of instantaneous power from the mechanical model agreed well with the power history used in the thermal model, independently inferred from thermocouple data. Axial shortening of the weld geometry required particular attention, and was handled by discarding thin layers of elements at discrete intervals to match the flash expulsion rate. The predicted distributions of plastic strain and heat generation were concentrated within narrow windows of temperature and flow stress, corresponding to a layer of material at the interface less than 1mm thick, consistent with weld micrographs.

1. Introduction

Linear friction welding is a solid state joining method, in which one component is subjected to reciprocating transverse motion against a stationary component, under axial compression. Four stages of the process were defined by Vairis and Frost [2] (Figure 1): *initial phase*: when heat is generated through sliding friction; *transition phase*: the formation of a plasticised layer and full contact; *equilibrium phase*: the plasticised material is expelled as flash, with axial shortening; and *deceleration and forge phase*, during which oscillations stop, under the axial forging pressure.

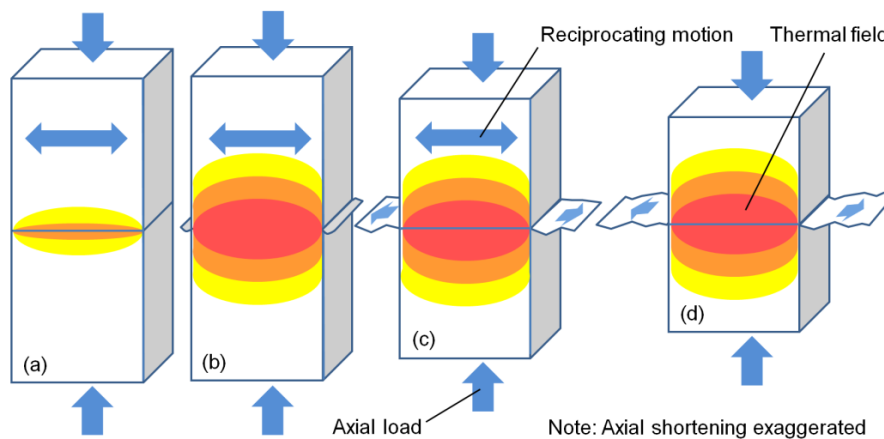


Figure 1 Linear friction welding: (a) initial phase, (b) transition phase, (c) equilibrium phase, (d) deceleration and forge phase (after [2]).

The process offers many of the metallurgical benefits of solid state friction welding, and has found commercial application in joining titanium alloy aero-engine compressor blades to disks. The LFW process, its application to Ti alloys, and the resulting properties have recently been reviewed in depth by McAndrew et al. [3]. A number of authors have studied LFW to examine the influence of welding parameters (amplitude, frequency, pressure and axial shortening) on: (i) the process operation (including temperature evolution, flash formation and defects, and residual stress); (ii) microstructure and texture in the weld zone, TMAZ and HAZ; and (iii) final mechanical properties (strength and ductility).

One of the important factors in LFW of Ti alloys is the phase transition between two different crystal structures: modified HCP α -Ti at lower temperatures, and BCC β -Ti at elevated temperatures, with the transition over a temperature range around 1000°C in the common Ti6Al4V alloy. Several processing characteristics and final properties have been tied to the $\alpha \rightarrow \beta \rightarrow \alpha$ transformations in LFW of Ti alloys [4]. For example, a high joint strength has been attributed to a refined microstructure, largely an outcome of rapid cooling of fully β transformed material [5,6]. Strong textures in the heavily deformed region adjacent to the bond-line were also attributed to the $\beta \rightarrow \alpha$ transformation in that region [7,8]. Microstructural observations [6] also suggested that temperatures exceeded the β -transus in the weld zone, but were below the β -transus in the TMAZ, which is consistent with the significant softening which occurs when α transforms to β .

Modelling of LFW

Numerical and occasional analytical modelling has been used to study all of the key aspects of the LFW process summarised above: the process operation, evolution of microstructure and properties, and their dependence on welding parameters (also reviewed for Ti LFW by McAndrew et al. [3]). The emphasis in the present work is on modelling the heat generation directly from the processing conditions and the constitutive behaviour of the material. The objectives of this are: (i) to improve the capability of FE modelling for predicting viable operating conditions for new component geometries and alloys, reducing the extent of empirical trials; (ii) to improve the definition of the input power history at the weld interface, as an essential input to predicting the temperature history and everything that flows from it (residual stress, and the evolution of microstructure and resulting properties). LFW modelling in the literature is reviewed here in two steps – first, to summarise the diverse goals of previous modelling on LFW, and second, to identify the key issues that need to be addressed in relation to modelling heat generation.

Some of the earliest work on LFW was by Vairis and Frost, who followed up their experimental investigations [2,9,10] with analytical and numerical models of LFW [11] predicting the temperature and frictional shear stress during the process. For computational efficiency, their model comprised a single deformable specimen in contact with a rigid body representing the second workpiece, with Coulomb friction between the two, varying with interface temperature. The model included work done in friction and plasticity, and model validation used average transverse force and temperature from a single thermocouple. Comparisons with other friction processes were handled in a similar fashion in the later work of Vairis et al. [12]. Temperature prediction forms a standard part of all subsequent modelling, often to relate weld temperatures to the α - β phase transformation. For example, from an FE analysis of LFW of Ti alloy in two conditions (β and $\alpha+\beta$), Sorina-Müller et al. [13] concluded that the weld interface reached the α - β transformation temperature, confirmed through microstructural analysis. Ji et al. [14] also developed a thermal model to inform their interpretation of LFW of Ti alloys with different starting microstructures. Thermal FE modelling to interpret microstructure evolution is not

limited to Ti alloys – Lis et al. [15] used a thermal model for LFW of 5000 and 6000 series Al alloys to derive relationships between weld hardness and temperature.

Understanding the transition from initial sliding to the full contact phase has been addressed empirically and numerically. For example, the group of Buffa, Fratini and co-workers [16-21] used experimentally measured forces and a finite element model of LFW in an iterative procedure to obtain a ‘shear coefficient’ – the ratio of the average shear stress at the interface to the material shear yield stress. The shear coefficient was variously explored as constant, temperature-dependent, or time-dependent. Schröder et al. [22,23] accounted for the transition from conditioning to equilibrium phase via an effective friction coefficient, with a heat input model derived from experimental force and velocity data. In their later work, Buffa et al. [24] used experimentally measured power directly as heat input in their thermal FE model, not only to derive the coefficient of friction for their thermomechanical models. Potet et al. [25] used an alternative method of estimating the frictional forces and heat input, calibrating the friction coefficient to match experimental thermocouple data and temperature predictions of their thermomechanical model.

In a series of papers, Li et al. have applied FE analysis to LFW, for carbon steels [26-29], Ni-based superalloys [30] and Ti alloy [31,32]. At the simplest level, these models were used to show that the interface temperature was relatively uniform, with a steep thermal gradient away from the interface. The temperature field was subsequently input for the prediction of residual stresses in LFW of Ti64 [32]. Their thermal analysis of cooling rates at the weld centre and flash root showed that much of the heat stored in the extruded flash is conducted back into the welded sample during the cooling stage [27]. They established empirical linear relationships between the heat generated and the welding parameters (frequency, amplitude and pressure), and correlated the heat input with the rate of axial shortening [31]. Similarly, McAndrew et al. [33,34] combined welding frequency and amplitude into a “rubbing velocity”, and used more elaborate statistical methods to build empirical equations relating amplitude, frequency and pressure to temperature, strain-rate and force at the interface, as well as burn-off rate, power, and the thickness of the TMAZ and flash. They used the statistical technique of analysis of variance, adopted later for similar purposes in the FE analysis by Effertz et al. [35].

Complex 3D thermomechanical models such as those of Li et al. also aim to capture the plastic strain fields in detail, with the objective of predicting the expulsion of flash and the rate of axial shortening. Similar methods have been developed for LFW of Ti6Al4V by McAndrew et al. [33,34,36,37], who accurately reproduced flash morphology with characteristic ridges observed experimentally – a particularly difficult modelling challenge [28], also carried out in high strength steel LFW by Effertz et al. [38,39]. Comparison between the size and shape of flash in an FE model and experiments was the sole validation method for the numerical simulation presented by Geng et al. [40]. The FE model built by Turner et al. [41] demonstrated the dependence of flash topology and strain-rates on the welding parameters, citing strain-rates of the order of 1000 s^{-1} in Ti6Al4V LFW. Other groups have built thermomechanical process models of LFW with similar objectives of examining the relationship between welding parameters, temperature distribution, and expulsion of the workpiece material – for example, Zhao et al. [42], Ji et al. [43] and Maio et al. [44] in Ti alloys, and Grujicic et al. in stainless steel [45,46] and in Ti alloy [47], with the latter authors including relevant microstructure evolution in both materials.

Turner et al.’s models were extended to predict residual stress fields on cooling, showing a strong correlation with the temperature distribution at the end of weld cycle [48]. On the other hand, the welding parameters and stress observed during the equilibrium stage were almost uncorrelated to residual stress. Song et al. [49] predicted residual stresses in LFW of Al alloys using a

thermomechanical FE model, and compared the predictions to experimental X-ray diffraction data. Buhr et al. [50,51] also predicted residual stress fields and validated them against neutron diffraction experiments. However, for computational efficiency they used a purely thermal process model, based on the work of McAndrew et al. [33,34,36].

Summary of key modelling issues

All of the thermomechanical models of LFW have in common a number of challenges: (a) choice of welding phase and interface boundary conditions: initial friction or bulk plasticity, or the transition between the two; (b) for modelling plastic deformation, the choice of suitable constitutive data for the material, and in Ti alloys the particular impact of the α - β transus; (c) the independent validation of the heat generation rate; (d) computational efficiency in a large-strain cyclic process such as LFW. The common options are outlined below, with the method(s) chosen by different authors summarised in Table 1.

Two approaches to modelling the interaction between joined components have been proposed: (i) specifying friction at the interface, and (ii) modelling both workpieces as a single part, with properties at the interface identical to those of the parent material. In its simplest form, the first approach relies on a calibrated or temperature-dependent coefficient of friction to account for the change of conditions at the welded interface. Frictional slip may also be replaced by a sticking regime with a limiting shear stress. The second approach covers only the equilibrium phase, after the workpieces have coalesced, allowing the joint to be modelled as a single part with bulk plasticity in the hot interface region.

Many authors have noted the importance of the temperature, strain-rate and strain dependencies of the material constitutive behaviour in governing and limiting the resulting temperature and deformation history in LFW, with a review of this aspect provided by Turner et al. [52]. The most common constitutive equation for flow stress adopted in LFW modelling is the Johnson-Cook model, or a similar empirical fit to hot flow stress data. Other authors argue that it is more robust to retain the raw flow stress as a function of temperature, strain-rate and strain in a tabular look-up form – even though this is less computationally efficient, it avoids the loss of precision in empirically fitted equations. Either approach assumes that the underlying hot deformation tests accurately deliver the response at a constant temperature and strain-rate, which is not straightforward given the effects of friction on test platens, heat dissipation by plastic deformation, and heat losses to the platens and air.

Several types of experimental results have been routinely used for model validation, as reviewed in [3]. The time variation of temperature is commonly measured, though this is challenging practically, given the difficulties of access and the steep thermal gradients near the weld interface. The measured axial shortening is commonly an input to the model, rather than a predicted output, closely related to the rate of flash expulsion. Some authors have used machine force data as a means to estimate the coefficient of friction, but few have been able to extract input power histories at the weld interface. Ofem et al. [53] demonstrated how this could be achieved, by allowing for machine inertia to separate the interface contact force from the force measured in the oscillation direction. This approach was used by the current authors [1], who compared experimental power obtained in this fashion, with the power history reverse-engineered from thermocouple data. This thermal FE model of LFW, with its independent estimates of power history, is used here for validation of the new deformation model.

To date, numerical modelling of LFW has been dominated by fully coupled thermomechanical finite element analysis with explicit time integration. Large deformations are commonly handled by an Arbitrary Lagrangian–Eulerian (ALE) kinematic description, or other remeshing techniques. The

computational effort associated with these approaches has been typically minimised by reducing the problem to two dimensions, or substituting one part with a rigid body – even so, many authors reported substantial computation times.

Table 1 Key modelling issues and approaches to their solution in the literature.

Modelling Issue	Approaches to the problem	References
Component interaction	Effective friction coefficient and/or limiting shear stress at the interface	Li et al. [27-29,31], Vairis and Frost [11], Buffa et al. [16-19,54], Fratini et al. [21], Ceretti et al. [20], Song et al. [49], Grujicic et al. [45-47], Ji et al. [14], Zhao et al. [42], Geng et al. [40], Potet et al. [25], Ji et al. [43], Maio et al. [44]
	Treating both workpieces as a single part	McAndrew et al. [33,34,36,37], Turner et al. [41,48], Schröder et al. [22,23], Effertz et al. [35,38,39]
Constitutive data	Johnson-Cook model (or similar empirical fit to data)	Li et al. [27-29,31], Song et al. [49], Grujicic et al. [45-47], Buffa et al. [17,18], Ji et al. [14], Vairis and Frost [11], Fratini et al. [21], Geng et al. [40], Ji et al. [43], Maio et al. [44]
	Tabulated experimental data	Turner et al. [41,48,52], McAndrew et al. [33,34,37], Zhao et al. [42] Effertz et al. [35,38,39], Potet et al. [25]
Independent validation of heat input	Inferred from machine forces and displacements	Ofem et al. [53], Jedrasiak and Shercliff [1], McAndrew et al. [33,34,36,37], Buffa et al. [16], Schröder et al. [22,23], Effertz et al. [38]
Computational efficiency in large strain LFW modelling	ALE kinematic description or other remeshing techniques	Li et al. [27-29,31], McAndrew et al. [33,34,37], Turner et al. [41,48], Buffa et al. [16,17,19], Song et al. [49], Grujicic et al. [45,47], Fratini et al. [21], Zhao et al. [42], Ceretti et al. [20], Schröder et al. [22,23], Potet et al. [25], Grujicic et al. [46]
	2D geometry	Li et al. [27,28], McAndrew et al. [33,34], Turner et al. [41,48], Song et al. [49], Effertz et al. [35,38], Ji et al. [14], Zhao et al. [42], Ceretti et al. [20], Schröder et al. [22,23], Maio et al. [44]
	Replacement of one part with a rigid body	Li et al. [27,31], Vairis and Frost [11], Buffa et al. [16,17,19], Ji et al. [14], Zhao et al. [42] Geng et al. [40], Potet et al. [25], Ji et al. [43], Maio et al. [44]

Small-strain analysis

All previous approaches to thermomechanical modelling of LFW are computationally intensive, since LFW involves both large strains and many deformation cycles. The aim of the current work is to advance a computationally efficient approach for modelling LFW, building on a methodology proposed for friction stir spot welding (FSSW) [55] and ultrasonic welding (USW) [56]. FSSW is characterised by large rotary plastic strains, while USW involves small strains per cycle, but very many deformation cycles, due to the high process frequency. The aspects of this methodology adapted to LFW are: (a) modelling the heat generation directly from a kinematic description of the workpiece interaction and the constitutive response of the alloy; (b) analysis of the heat generation through multiple small strain analyses as ‘snapshots’ within the large strain process; (c) modelling the heat flow and temperature field continuously throughout the process, but only finding the heat generation from single deformation cycles, at intervals through the weld time. By decoupling the timescales of the intensive deformation model from the fast thermal model, and using small strain analysis, the resulting model is computationally efficient.

Figure 2 illustrates the underlying concept behind the small strain method. Within each cycle (time step), the temperature field from the thermal model (Figure 2b) is imposed as an input to the deformation

model, while the heat generation rate distribution from the deformation model (Figure 2c) becomes an input load in the thermal model. The main novelty lies in the deformation model, which takes periodic ‘snapshots’ of the plastic heat dissipation at an instant, over a much shorter timescale than the interval between deformation analyses, but sufficient to capture the plastic strain-rate distribution. This power distribution is applied over the longer timescale of the thermal model, updating the temperature field, and the cycle repeats. The assumption is therefore that heat flow evolves over much longer timescales than deformation. There are two main sources of computational efficiency – firstly, the deformation model simulates only a small fraction of the total process time; and secondly, the strain and mesh distortions are small, so that the demanding kinematic description and remeshing associated with large strains can be avoided. The basic procedure is shown in Figure 2.

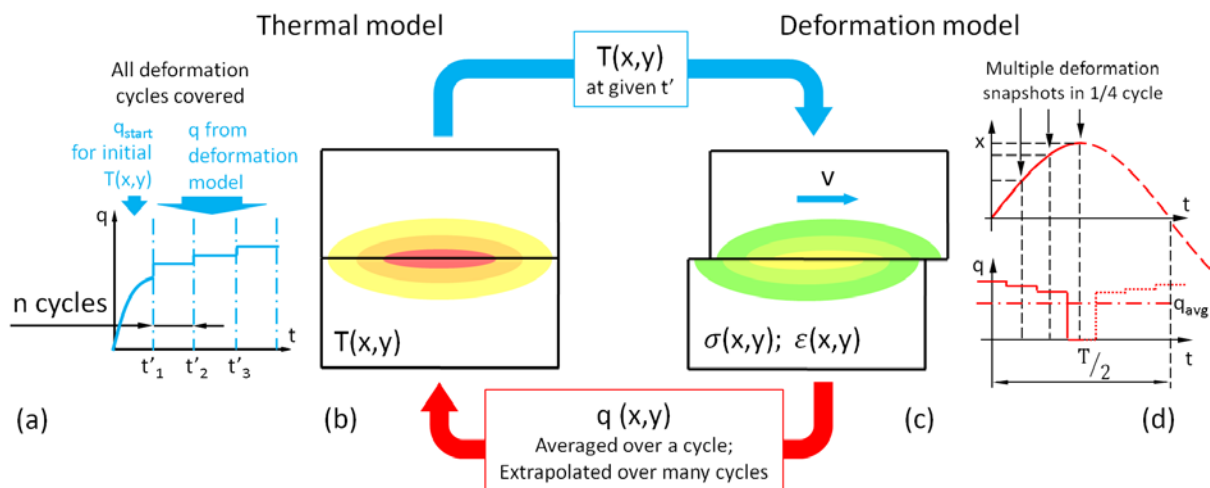


Figure 2 Small strain analysis of linear friction welding: (a) heat input history; (b) thermal model; (c) deformation model; (d) workpiece velocity

The small-strain finite element ‘snapshot’ approach has proven to be a reliable, computationally efficient method when modelling FSSW of Al and Mg alloys [55]. Here, the method is applied to linear friction welding of Ti6Al4V alloy, which tests its applicability to large strain, high-temperature, cyclic plastic deformation, with an evolving geometry (due to burn-off). As a proof-of-concept, the model is applied to the equilibrium stage of LFW, once full contact is established between the workpieces.

2. Experimental Work

Experimental data for this modelling work was obtained from instrumented LFW conducted at TWI Cambridge by collaborating researchers – the details are presented in a previous paper [1]. As a test case of the new small-strain approach to modelling LFW, the results are presented for a single set of welding parameters: 50Hz frequency, 2.7mm oscillation amplitude, downforce of 100kN and 3mm burn-off. The workpieces were made of two-phase α - β Ti-6Al-4V, with the geometry shown in Figure 3. Temperature was measured with four k -type thermocouples, inserted into drilled holes and fixed using an epoxy resin, using a data sampling rate of 1000Hz.

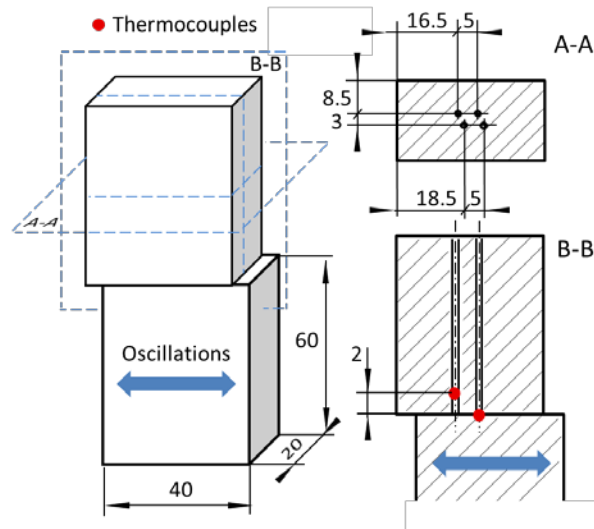


Figure 3 Joint dimensions (the same dimensions, in mm, for both workpieces). Thermocouple locations shown in the two sections A-A, B-B, at distances of 0, 0.5, 1.5 and 2mm from the interface.

Forces and displacements were measured in both oscillation and axial directions. As discussed earlier, these data were used to estimate the contribution from machine inertia and hence the interface force and power input [1]. Difficulties with data sampling rate and small phase shifts between the recorded signals limited the accuracy of this estimate, but the form of the power history with time were consistent with those inferred by thermal modelling, as illustrated below.

3. Thermal modelling

The finite element model for the thermal field is presented in [1], and outlined here as far as it impacts on the deformation model. The thermal model is two-dimensional, as the heat flow was practically one-dimensional in the axial direction, while the plastic deformation takes place through shearing in a thin layer at the welded interface, parallel to the oscillations. Due to the low thermal conductivity of titanium and the short welding cycle (of order 1s), the heat flow distance during the weld cycle is limited in extent. Hence the initial dimensions of the workpieces were limited to 10mm, and remaining parts of the workpieces and clamping could be neglected. For the same reasons, heat losses to the air were neglected, with perfect thermal contact between the workpieces.

In the initial stage of LFW, the weld interface at the edges is in intermittent contact over a distance equal to the oscillation amplitude. The extreme edge of the workpiece is exposed to the air for half of the cycle, which leads to a taper in the heat input at the edge to half the value associated with the area of full contact [1]. Since the amplitude is less than 7% of the workpiece length, the extent of this edge effect is modest. Once the interface is in full contact in the equilibrium stage, hot deforming flash replaces the air contact, and the edge effect is significantly reduced – hence it is reasonable in the current context to neglect this edge effect, and to assume that the deformation and resulting heat input distribution is uniform over the entire weld interface. A uniform heat input is also reasonable since, over the dominant area of continuous full contact, the temperature field only varies axially, while the kinematic constraint imposes a uniform strain-rate distribution in the transverse direction. The oscillation leads to cyclic deformation at the interface, but given the high oscillation frequency, the heat generation may be averaged over a cycle and applied as a continuous input during the overall welding time, in order to predict the temperature field. The net power history input, $q(t)$, was adjusted empirically with a piece-wise linear variation. At each time-step, the power was adjusted iteratively until the model matched the measured temperature for the thermocouple closest to the interface. As

burn-off reached the location of each thermocouple, the data from that thermocouple could no longer be trusted, and calibration switched to the next closest thermocouple, and so on.

One particularly challenging aspect of modelling LFW with the proposed small-strain framework is the need for handling the change of geometry associated with burn-off. Figure 4 illustrates how this was achieved, by deleting layers of elements at the interface at intervals, closing up the model each time on the plane of symmetry at the joint interface. Each layer of elements corresponded to an equivalent volume of material extruded to flash in the same time interval, that is, the removal rate of layers of elements was matched with the experimentally measured burn-off.

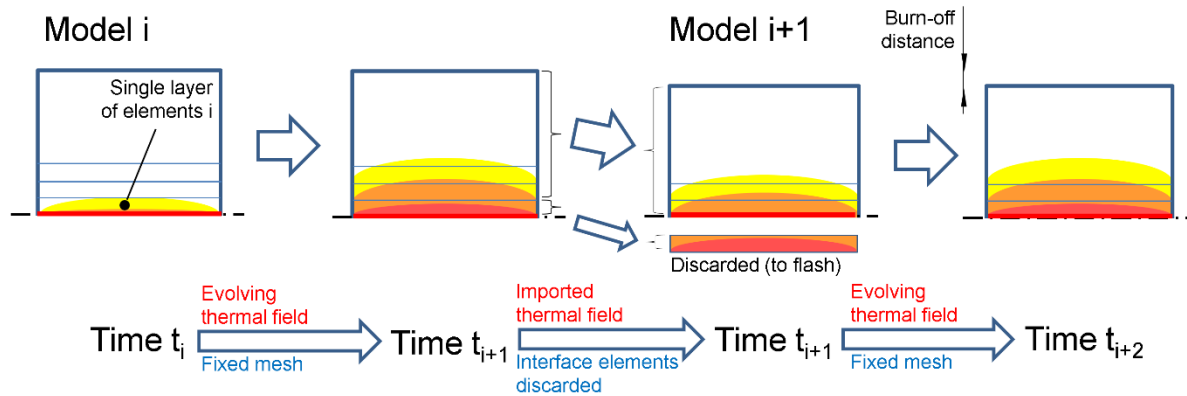


Figure 4 Iterative axial shortening in the thermal model.

The power history inferred from the thermal model is shown in Figure 5, together with the temperature predictions compared with the thermocouple data, up to the point when the thermocouples entered the deformation zone. The results are sensitive to the thermocouple locations, due to the steep temperature gradient. The power input also showed some scatter due to the sequential treatment of the burn-off process (which could be reduced by a decrease in mesh size and more frequent burn-off steps). The power history in Figure 5 is a smoothed best fit, but has an estimated uncertainty of order $\pm 20\%$.

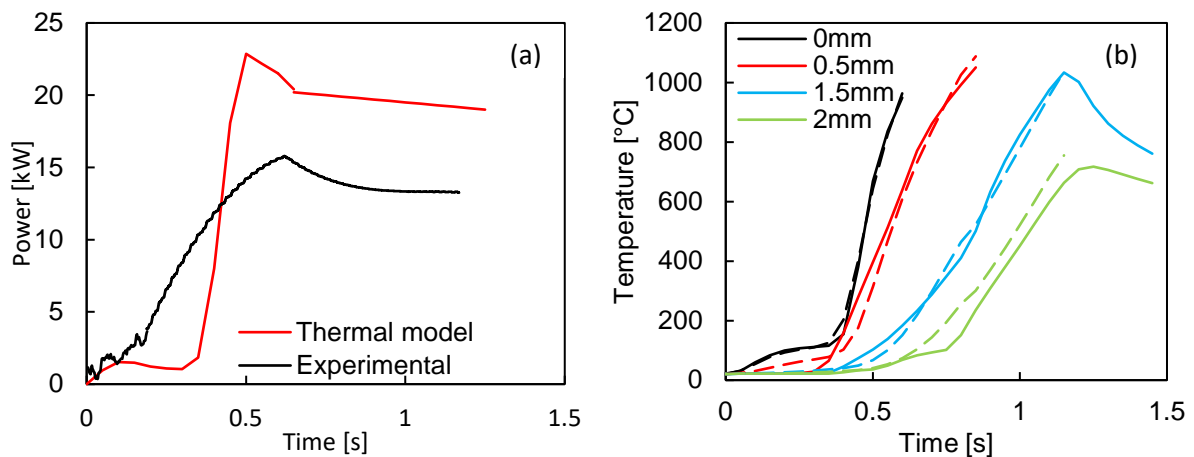


Figure 5 (a) Predicted power history inferred from the thermal model; (b) corresponding temperature histories (dashed lines) and thermocouple data (solid lines), for given (initial) distances from the interface.

4. Deformation modelling

The goal of the deformation model is to find a computationally efficient method for estimating the power history directly from the constitutive behaviour of the material and the process kinematics. As outlined in Figure 2, the proposed small-strain approach achieves this by decoupling intermittent snapshot deformation analyses from the much longer timescale of the thermal analysis.

Material constitutive data

Material elastic properties for Ti-6Al-4V alloy were specified as temperature-dependent [57] while the constitutive flow stress data included temperature and strain-rate dependency. Figure 6 shows a set of best-fit curves, using data derived from experimentally measured stress-strain curves, as a function of temperature and strain-rate [41]. The prevailing conditions in the equilibrium stage in LFW are for large strain deformation at temperatures and strain-rates where there is no strain-dependence. Lower temperature data showed some work hardening so, for completeness of the input data, the yield stress in all cases was taken at the maximum available strain. The data plotted in Figure 6 were fitted using a polynomial and the least square method to approximate the temperature-dependence curve at a mid-range strain-rate, and then by assuming linear dependence between flow stress and $\log(\text{strain-rate})$. Note the softer response above the α - β transition (that is, above 900-1000°C in Ti6Al4V alloy), though the onset of significant softening appears to be around 600-700°C.

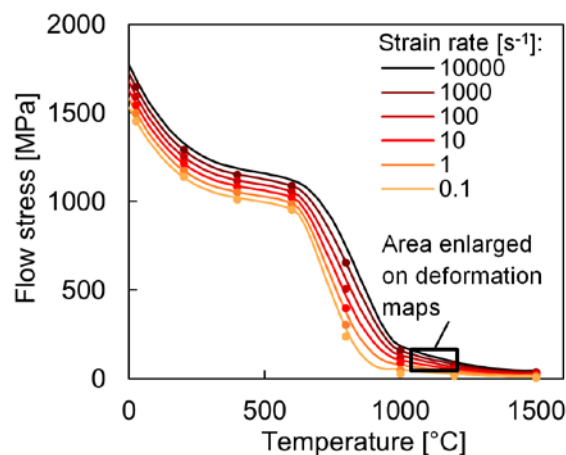


Figure 6 Flow stress of Ti-6Al-4V (datapoints – experimental data, solid lines – model) [41]
(The highlighted region is shown enlarged in a later material deformation map, Fig. 14).

Finite element mesh and kinematic boundary conditions

The deformation model imports the temperature field on a node-by-node basis, and this is assumed unchanged throughout a single deformation cycle. Note that the mechanical analyses are conducted every 5 cycles, while the burn-off steps in the thermal model are applied at intervals determined independently using the experimental burn-off rate. The deformation and power analyses therefore fall arbitrarily at intervals between the burn-off steps in the thermal model, as shown in Figure 7. The dimensions and mesh of both workpieces in the deformation model is therefore identical to the current mesh in the thermal model.

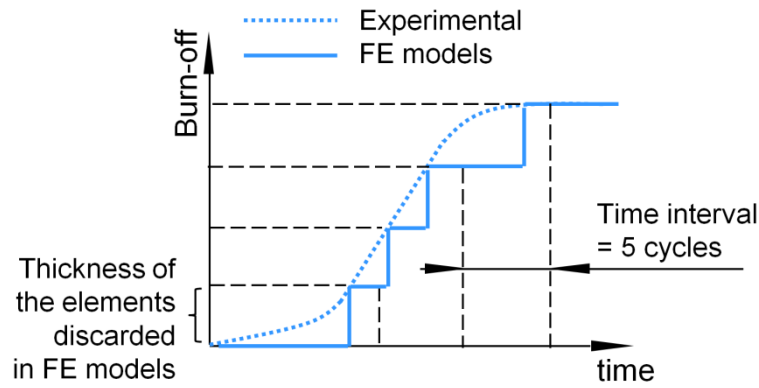


Figure 7 Axial shortening as a function of time in the small-strain LFW model.

Figure 8 shows the mesh for a typical snapshot deformation analysis. All the degrees of freedom of the bottom surface of the lower (stationary) workpiece are fixed. The top surface of the upper (oscillating) workpiece is constrained to move laterally, with the vertical direction unconstrained. The top rigid surface is subjected to a vertical downforce F which is evenly distributed over the width of the workpiece, giving a uniform interface pressure. Each deformation analysis starts at a prescribed offset in the upper workpiece (x) with nodes from one surface being constrained to have the same motion as the closest point at the other surface (global displacements and rotations as well as all other active degrees of freedom are equal at nodes on both sides of the interface). In each analysis, a small horizontal displacement Δx is imposed at a constant velocity (of a magnitude defined below).

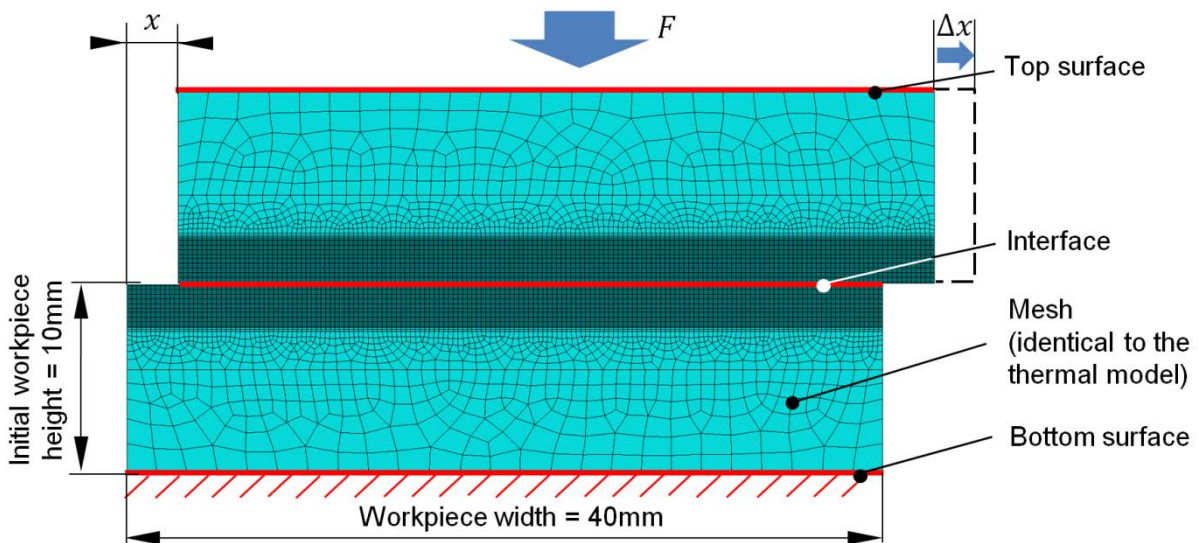


Figure 8 LFW deformation model – geometry, mesh, loads and boundary conditions.

In LFW, the oscillation amplitude is relatively large compared to the thickness of the deforming layer (of order 2-3mm). As a consequence, if an entire cycle were modelled, the deformation would result in excessive distortion of the Lagrangian mesh. To cope with this, a single cycle is simulated with several small-strain models, each covering a snapshot of the deformation, at different points in the cycle. Figure 9 illustrates the concept, identifying a number of key timescales. First, individual oscillation cycles are considered, at time intervals (t_j, t_{j+1} , etc) corresponding to many oscillations (Figure 9a). The power generated by each cycle may actually be predicted from analysis of a quarter cycle (since the range of motion and plastic dissipation is identical in each quarter cycle). A typical quarter-cycle starting at time t_j is illustrated in Figure 9b: the quarter-cycle is simulated with three small-strain snapshot models,

uniformly spaced at times t_j , t_j' , and t_j'' (noting that the workpiece is stationary at t_j'''). At the start of each snapshot model, the relative position is first imposed, with $x(t) = 0.9\text{mm} \times i$ (for $i = 0$ to 2, with no analysis being necessary for $i = 3$ when the offset is equal to the amplitude of 2.7mm, when there is no motion). The instantaneous velocity at each $x(t)$ is known from the instantaneous gradient of the sinusoidal $x(t)$ cycle (illustrated for time t_j' in Figure 9c). In each snapshot, the small displacement Δx is applied at this constant velocity, $\frac{\Delta x}{\Delta t}$. The analysis therefore includes a number of different timescales – Table 2 summarises the values used for the weld in this study.

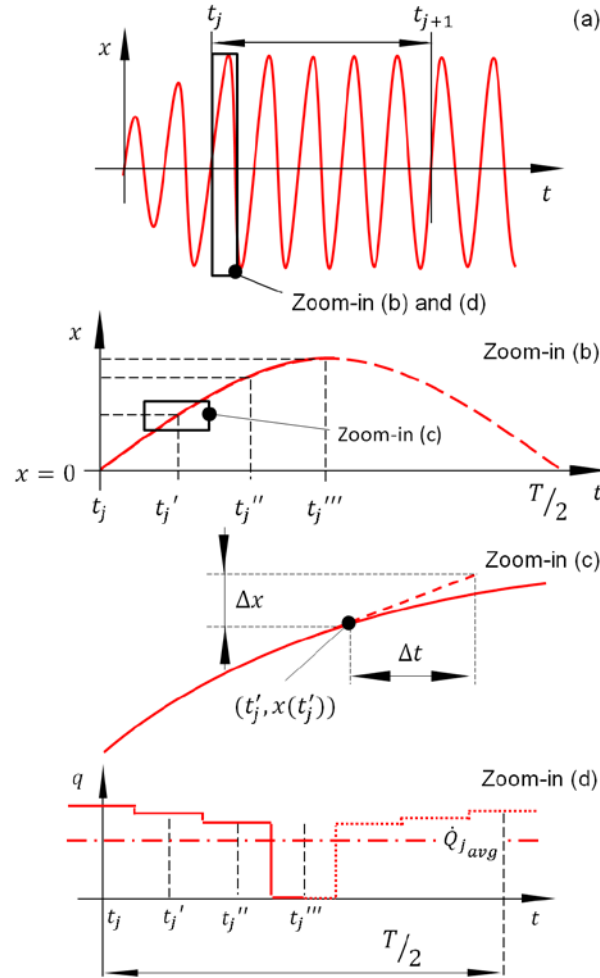


Figure 9 Displacement $x(t)$, defining the timescales of the deformation model: (a) selected oscillation cycles during the weld; (b) quarter-cycle of a single oscillation; (c) single snapshot model. The process for averaging the power prediction over half a cycle is shown in (d).

Variable		Value
Oscillation period	T	0.02s
Time increment between quarter-cycle analyses	$t_{j+1} - t_j$	0.1s ($= 5T$)
Time increment between snapshot models within quarter cycle	$t_j' - t_j$	0.0017s ($= T/12$)
Duration of snapshot analysis	$\Delta t = \Delta x/v(t)$	variable ($\Delta x = 0.1\text{mm}$)

Table 2 Summary of timescales shown in deformation analysis.

The displacement $\Delta x = 0.1\text{mm}$ imposed in each snapshot model need to be small enough to avoid substantial mesh distortion, while capturing the plastic deformation within the real continuous cyclic process. The model displacement is initially accommodated by elastic deformation, but is continued until a constant plastic strain-rate is established, with a corresponding rate of plastic power dissipation (Figure 10).

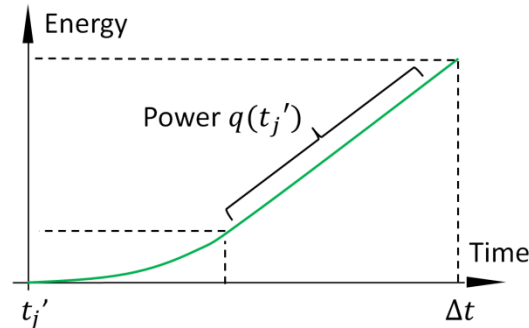


Figure 10 Heat generation as a function of time for a typical snapshot model, showing the transition to a constant plastic dissipation rate.

The plastic work-rates for each of the snapshots are then averaged over half a cycle, as follows. First the values of the instantaneous power are associated with a time interval *centred* on the start time of each snapshot calculation (t_j , t_j' , and t_j'' , and zero power at t_j'''), to minimise the error between actual time-varying and constant piecewise values. The power is assumed to vary stepwise, as shown in Figure 9(d), with the following quarter-cycle being a mirror image, and the plastic dissipation is then averaged over a half-cycle. The accuracy could naturally be improved if the number of time steps in a quarter cycle were increased.

Results

The power predictions from the small-strain snapshot model are compared with the power inferred from the thermal model in Figure 11. The power predicted by the deformation model is about 20% higher than that from the thermal model, and showed a systematic variation with a shallow minimum in the middle of the equilibrium stage. The steep temperature gradient led to uncertainty in the thermal model, but also influences the deformation model through the temperature-sensitivity of the flow stress. It is difficult therefore to resolve the discrepancy in magnitude or shape of the power variation, given the accumulated uncertainties in the models. The uncertainty could be reduced by: (i) refining the mesh, to enable more frequent burn-off steps; (ii) an increase in the number of snapshot analyses per quarter cycle; (iii) refinement of the constitutive data; (iv) validation against a wider range of welding conditions. But overall, the agreement between the power variation using the two models suggests that the methodology provides a sound computationally efficient method for predicting the power directly from the constitutive response, to an accuracy of better than 20%. Given the cost of experimental trials, this offers potential benefits in selecting initial trial conditions, particularly for application of LFW to new alloys (such as aerospace Al alloys).

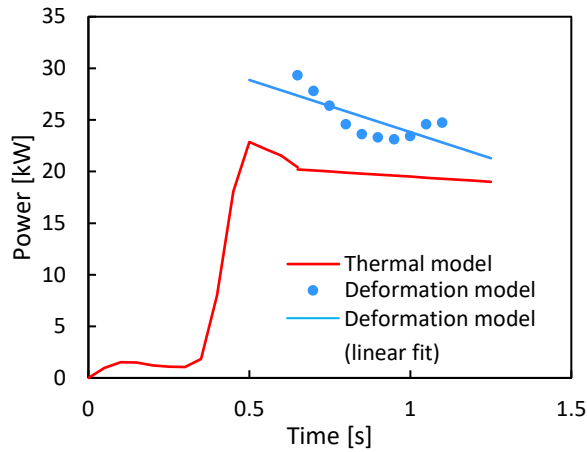


Figure 11 Predicted heat generation rate vs time from the deformation model (blue), and reverse engineered from thermocouple data using the thermal model (red).

To provide further insight into the material deformation, contour maps of heat generation rate (per unit volume) and equivalent plastic strain are shown for the end of the equilibrium stage in Figure 12(a,b). Note that the extent of deformation is predicted to be less than 0.5mm to either side of the interface (compared to a workpiece width of 40mm). The micrograph of a weld cross-section (Figure 12c) shows that the experimentally measured extent of the TMAZ closely matches the model prediction.

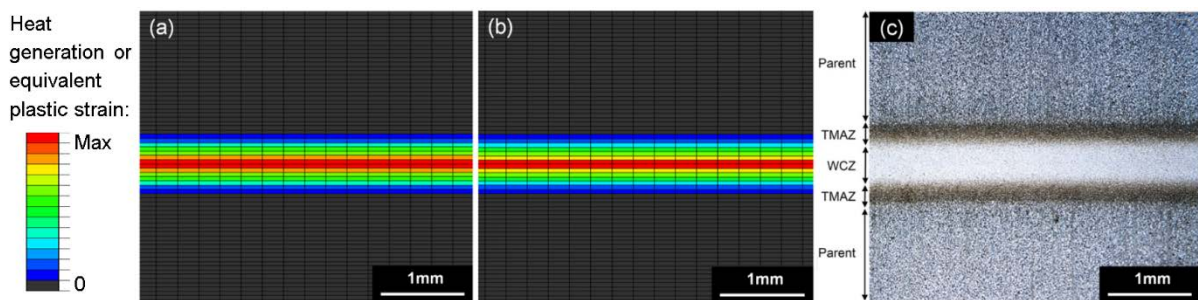


Figure 12 Cross-section through the weld at the beginning of the equilibrium stage:

- (a) predicted distribution of heat generated per unit volume close to the interface;
- (b) corresponding equivalent plastic strain at the interface;
- (c) experimental weld cross-section showing weld zone (WCZ) and thermomechanically affected zone (TMAZ).

Material deformation maps

An approach to visualisation of the material deformation behaviour, which has proven to give valuable insight, was proposed by Colegrove et al. in their work on CFD modelling of FSW [58, 59]. The method is to take the plot of flow stress as a function of temperature and strain-rate, and to overlay contours showing the probability that material will experience the underlying deformation conditions. These ‘material deformation maps’ highlight the dominant temperature and strain-rate regime for the plastic regions in FS welds. This approach helps to understand material softening behaviour, and can be a practical tool for selection of parameter windows or alloys with a desirable constitutive behaviour. The present work modifies this approach, displaying the *amount of heat* generated in a given set of material conditions, rather than the probability that they will occur. Deformation conditions during each application of the heat generation model are interrogated increment-by-increment and element-by-element (Figure 13a), with the heat generated in each element being sorted into “bins” defined by given ranges of flow stress and temperature (Figure 13b). The final total in each bin is expressed as a fraction

of the total heat input to the weld in that deformation step, and these are superimposed as contours on the flow stress-temperature plot (Figure 13c).

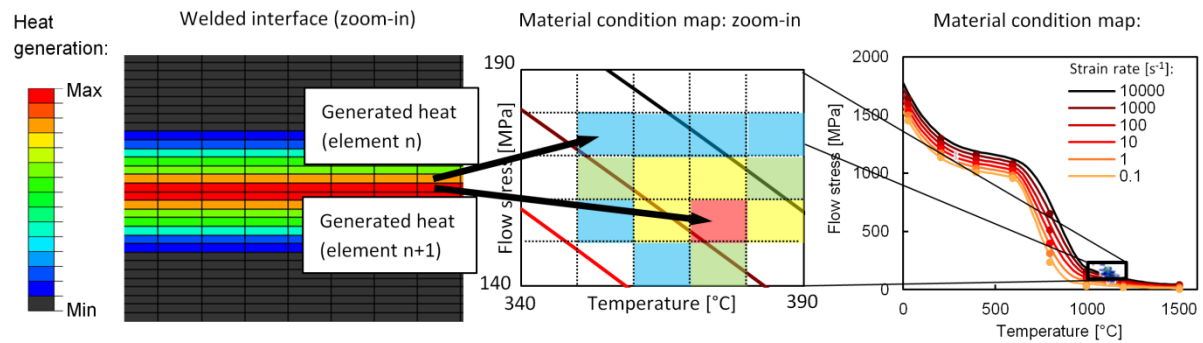


Figure 13 Mapping heat generation onto constitutive data in a material deformation map.

Figure 14 shows these maps for 3 weld times on an enlarged region of the flow stress – temperature plot. In each case the deformation is concentrated within narrow temperature and flow stress bounds, where the flow stress is practically constant, and the temperature varies by around 20°C. The predicted strain-rates in the deformation zone lie in the range 1500-5000 s⁻¹, which is somewhat higher but of similar order to values cited in more complex models [33]. The analysis also indicates that welding operates above the $\alpha \rightarrow \beta$ transition temperature, in the region where the flow stress is relatively low. So this transition is critical in friction welding of titanium. Above that temperature the process achieves a near steady-state, in which the heat generated balances the heat conducted away from the joint line, maintaining constant temperature and deformation conditions. Deformation at temperatures below $\alpha \rightarrow \beta$ leads to a high flow stress, generating more heat than necessary to maintain equilibrium. That leads to increasing temperatures and decreasing flow stress, until the conditions from Figure 14 are achieved. This creates a self-limiting process, where temperatures will always tend to a certain range above the $\alpha \rightarrow \beta$ transus. During an idealized equilibrium stage, deformation conditions self-stabilize, and depend on the welding parameters and material characteristics.

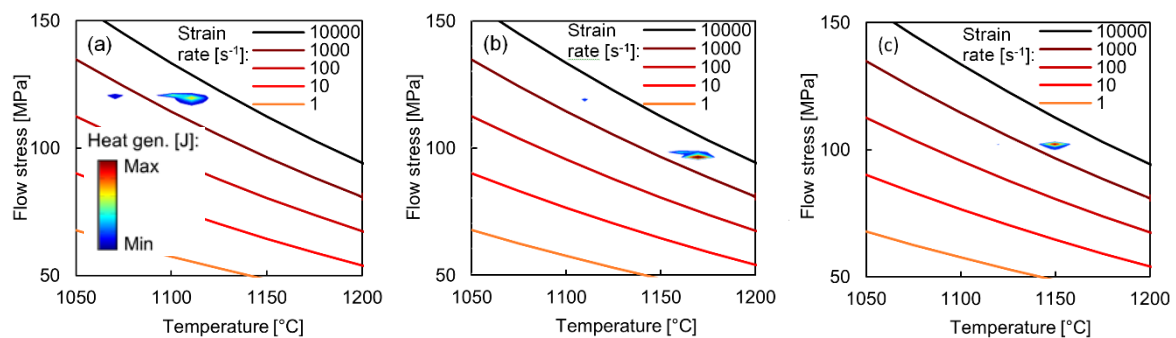


Figure 14 Material condition maps showing flow stress of Ti6Al4V as a function of temperature and strain rate, with the dominant conditions for heat generation in a linear friction welding at weld times of (a) 0.65s (beginning of equilibrium stage); (b) 0.85s; and (c) 1s (end of equilibrium stage).

5. Conclusions

This paper successfully applied a computationally efficient small-strain thermomechanical modelling approach to the linear friction welding of Ti alloy, testing the concept on the equilibrium stage. The specific techniques developed in this approach, and the principal outcomes, are:

- i. A continuous two-dimensional thermal model of LFW [1] was coupled to a thermomechanical model running at discrete intervals during welding – this limits the computationally intensive analysis to a small proportion of the welding time.
- ii. Each run of the thermomechanical model analyses only a single quarter-cycle of the oscillation, with a number of small-strain analyses during this interval, giving a faster computation by avoiding distortion of the mesh. The plastic work-rates obtained during each quarter-cycle analysis were then time-averaged to give the power over one cycle at that time during the welding process.
- iii. The expulsion of the material to flash and associated burn-off were taken into account by progressively deleting layers of elements, enabling continuous prediction of the temperature field for input to the deformation model.
- iv. The power history was predicted directly from a kinematic description of the workpiece motion and the material constitutive response, and the agreement was reasonable with that inferred independently from the thermal model (given the uncertainties in the constitutive data and the thermocouple measurements). The predicted width of the deformation zones was close to that seen in a micrograph of the weld cross-section.
- v. Further insight was gained via material deformation maps, which indicated that the deformation was concentrated within narrow ranges of temperature and flow stress.

Acknowledgements

The work described in this paper was funded by the UK Engineering and Physical Sciences Research Council (EPSRC) through the University of Cambridge Doctoral Training Account, with additional CASE award funding provided by TWI, Granta Park, Cambridge, UK, where funding for the experiments was provided by the Boeing Corporation. The work was completed for publication under the EPSRC programme grant EP/R001715/1 (LightForm: Embedding Materials Engineering in Manufacturing with Light Alloys). The authors gratefully acknowledge the technical discussions and experimental collaboration with Dr. Anthony McAndrew and Dr. Paul Colegrove of the University of Cranfield, and Dr Mike Russell, Dr Kathryn Beamish and Bertrand Flipo, of TWI Cambridge.

Declarations of interest

None.

Data availability

The raw/processed data required to reproduce these findings cannot be shared at this time due to technical or time limitations.

References

- [1] P. Jedrasiak, H.R. Shercliff, A.R. McAndrew, P.A. Colegrove, "Thermal Modelling of Linear Friction Welding," *Materials & Design*, vol. 156, pp. 362-369, 2018.
- [2] A. Vairis, M. Frost, "High frequency linear friction welding of a titanium alloy," *Wear*, vol. 217, pp. 117-131, 1998.
- [3] A.R. McAndrew, P.A. Colegrove, C. Bühr, B.C.D. Flipo, A. Vairis, "A literature review of Ti-6Al-4V linear friction welding," *Progress in Materials Science*, vol. 92, pp. 225-257, 2018.

- [4] M. Peters, J. Hemptenmacher, J. Kumpfert, C. Leyens, "Structure and Properties of Titanium and Titanium Alloys," in *Titanium and Titanium Alloys: Fundamentals and Applications*, Weinheim, Wiley-VCH, 2003, pp. 1-36.
- [5] I. Bhamji, M. Preuss, P.L. Threadgill, A.C. Addison, "Solid state joining of metals by linear friction welding: A literature review," *Materials Science & Technology*, vol. 27, no. 1, pp. 2-12, 2010.
- [6] P. Wanjara, M. Jahazi, "Linear friction welding of Ti-6Al-4V: Processing, microstructure, and mechanical-property inter-relationships," *Metallurgical and Materials Transactions A - Physical metallurgy and materials science*, vol. 36A, no. 8, pp. 2149-2164, 2005.
- [7] M. Karadge, M. Preuss, C. Lovell, P.J. Withers, S. Bray, "Texture development in Ti-6Al-4V linear friction welds," *Materials Science and Engineering A - Structural Materials Properties Microstructure and Processing*, vol. 459, no. 1-2, pp. 182-191, 2007.
- [8] M. Karadage, M. Preuss, P.J. Withers, S. Bray, "Importance of crystal orientation in linear friction joining of single crystal to polycrystalline nickel-based superalloys," *Materials Science and Engineering A: Structural Materials: Properties, Microstructure and Processing*, vol. 491, no. 1-2, p. 446-453, 2008.
- [9] A. Vairis, M. Frost, "On the extrusion stage of linear friction welding of Ti6Al4V," *Materials Science and Engineering A - Structural Materials Properties Microstructure and Processing*, vol. 271, no. 1-2, pp. 477-484, 1999.
- [10] A. Vairis, "Investigation of frictional behaviour of various materials under sliding conditions," *European Journal of Mechanics - A/Solids*, vol. 16, no. 6, pp. 929-945, 1997.
- [11] A. Vairis, M. Frost, "Modelling the linear friction welding of titanium blocks," *Materials Science and Engineering: A*, vol. 292, no. 1, p. 8-17, 2000.
- [12] A. Vairis, G. Papazafeiropoulos, A.M. Tsainis, "A comparison between friction stir welding, linear friction welding and rotary friction welding," *Advances in Manufacturing*, vol. 4, no. 4, pp. 296-304, 2016.
- [13] J. Sorina-Müller, M. Rettenmayr, D. Schneefeld, O. Roder, W. Fried, "FEM simulation of the linear friction welding of titanium alloys," *Computational Materials Science*, vol. 48, p. 749-758, 2010.
- [14] Y. Ji, Z. Chai, D. Zhao, S. Wu, "Linear friction welding of Ti-5Al-2Sn-2Zr-4Mo-4Cr alloy with dissimilar microstructure," *Journal of Materials Processing Technology*, vol. 214, p. 979-987, 2014.
- [15] A. Lis, H. Mogami, T. Matsuda, T. Sano, R. Yoshida, H. Hori, A. Hirose, "Hardening and softening effects in aluminium alloys during high-frequency linear friction welding," *Journal of Materials Processing Technology*, vol. 255, pp. 547-558, 2018.
- [16] G. Buffa, M. Cammalleri, D. Campanella, L. Fratini, "Shear coefficient determination in linear friction welding of aluminum alloys," *Materials & Design*, vol. 82, p. 238-246, 2015.
- [17] G. Buffa, D. Campanella, S. Pellegrino, L. Fratini, "Weld quality prediction in linear friction welding of AA6082-T6 through an integrated numerical tool," *Journal of Materials Processing Technology*, vol. 231, pp. 389-396, 2016.
- [18] D. Baffari, G. Buffa, D. Campanella, L. Fratini, F. Micari, "Single block 3D numerical model for linear friction welding of titanium alloy," *Science and Technology of Welding and Joining*, vol. 24, no. 2, pp. 130-135, 2019.

- [19] G. Buffa, S. Pellegrino, E. Lo Valvo, L. Fratini, "Comparative analysis of bonding mechanism in solid state metal working processes," in *NUMIFORM 2016: 12th International Conference on Numerical Methods in Industrial Forming Processes*, Université de technologie de Troyes, Troyes, FRANCE, 2016.
- [20] E. Ceretti, L. Fratini, C. Giardini, D. La Spisa, "Numerical modelling of the linear friction welding process," *The International Journal of Material Forming*, vol. 3, pp. 1015-1018, 2010.
- [21] L. Fratini, G. Buffa, D. Campanella, D. La Spisa, "Investigations on the linear friction welding process through numerical simulations and experiments," *Materials & Design*, vol. 40, pp. 285-291, 2012.
- [22] F. Schröder; R.M. Ward; A.R. Walpole; R.P. Turner; M.M. Attallah; J.C. Gebelin; R.C. Reed, "Linear friction welding of Ti6Al4V: experiments and modelling," *Materials Science and Technology*, vol. 31, no. 3, pp. 372-384, 2015.
- [23] F. Schroeder; R.M. Ward; R.P. Turner; A.R. Walpole; M.M. Attallah; J.C. Gebelin; R.C. Reed, "Validation of a Model of Linear Friction Welding of Ti6Al4V by Considering Welds of Different Sizes," *Metallurgical and Materials Transactions B: Process Metallurgy and Materials Processing Science*, vol. 46, no. 5, pp. 2326-2331, 2015.
- [24] G. Buffa, M. Cammalleri, D. Campanella, U. LaCommare, L. Fratini, "Linear friction welding of dissimilar AA6082 and AA2011 aluminum alloys: microstructural characterization and design guidelines," *International Journal of Material Forming*, vol. 10, no. 3, p. 307–315, 2017.
- [25] A. Potet, K. Mocellin, L. Fourment, "Numerical simulation of linear friction welding of aeronautical alloys," in *Proceedings of the 20th International ESAFORM Conference on Material Forming: ESAFORM 2017*, Dublin City University, Dublin, Ireland, 2017.
- [26] W.Y. Li; T.J. Ma; S.Q. Yang; Q.Z. Xu; Y. Zhang; J.L. Li; H.L. Liao, "Effect of friction time on flash shape and axial shortening of linear friction welded 45 steel," *Materials Letters*, vol. 62, no. 2, pp. 293-296, 2008.
- [27] W.Y. Li, S.X. Shi, F.F. Wang, T.J. Ma, J.L. Li, D.L. Gao, A. Vairis, "Heat reflux in flash and its effect on joint temperature history during linear friction welding of steel," *International Journal of Thermal Sciences*, vol. 67, pp. 192-199, 2013.
- [28] W.Y. Li, F.F. Wang, S.X. Shi, T.J. Ma, "Numerical Simulation of Linear Friction Welding Based on ABAQUS Environment: Challenges and Perspectives," *Journal of Materials Engineering and Performance*, vol. 23, no. 2, pp. 384-390, 2014.
- [29] W.Y. Li, F.F. Wang, S.X. Shi, T.J. Ma, J.L. Li, A. Vairis, "3D Finite Element Analysis of the Effect of Process Parameters on Linear Friction Welding of Mild Steel," *The Journal of Materials Engineering and Performance*, vol. 23, no. 11, pp. 4010-4018, 2014.
- [30] X. Yang, W. Li, J. Li, B. Xiao, T. Ma, Z. Huang, J. Guo, "Finite element modeling of the linear friction welding of GH4169 superalloy," *Materials and Design*, vol. 87, p. 215–230, 2015.
- [31] W.Y. Li, T.J. Ma, J.L. Li, "Numerical simulation of linear friction welding of titanium alloy: Effects of processing parameters," *Materials & Design*, vol. 31, no. 3, pp. 1497-1507, 2010.
- [32] Y. Fu, W.Y. Li, X.W. Yang, T.J. Ma, A. Vairis, "The effects of forging pressure and temperature field on residual stresses in linear friction welded Ti6Al4V joints," *Advances in Manufacturing*, vol. 4, no. 4, pp. 314-321, 2016.
- [33] A.R. McAndrew, P.A. Colegrove, A.C. Addison, B.C.D. Flipo, M.J. Russell, "Modelling the influence of the process inputs on the removal of surface contaminants from Ti-6Al-4V linear friction welds," *Materials & Design*, vol. 66A, p. 183–195, 2015.

- [34] A.R. McAndrew, P.A. Colegrove, A.C. Addison, B.C.D. Flipo, M.J. Russell, "Energy and Force Analysis of Ti-6Al-4V Linear Friction Welds for Computational Modeling Input and Validation Data," *Metallurgical and Materials Transactions A - Physical metallurgy and materials science*, vol. 45A, no. 13, pp. 6118-6128, 2014.
- [35] P.S. Effertz, F. Fuchs, N. Enzinger, "The influence of process parameters in linear friction welded 30CrNiMo8 small cross-section: a modelling approach," *Science and Technology of Welding and Joining*, vol. 24, no. 2, pp. 121-129, 2019.
- [36] A.R. McAndrew, P.A. Colegrove, A.C. Addison, B.C.D. Flipo, C.D. Bertrand, M.J. Russell, L.A. Lee, "Modelling of the workpiece geometry effects on Ti-6Al-4V linear friction welds," *Materials & Design*, vol. 87, pp. 1087-1099, 2015.
- [37] A.R. McAndrew, P.A. Colegrove, B.C.D. Flipo, C. Bühr, "3D modelling of Ti-6Al-4V linear friction welds," *Science and Technology of Welding and Joining*, vol. 22, no. 6, p. 496-504, 2017.
- [38] P.S. Effertz, F. Fuchs, N. Enzinger, "Modelling the flash formation of linear friction welded 30CrNiMo8 high strength steel chains," *The International Journal of Advanced Manufacturing Technology*, vol. 92, no. 5-8, p. 2479-2486, 2017.
- [39] P.S. Effertz, F. Fuchs, N. Enzinger, "3D Modelling of Flash Formation in Linear Friction Welded 30CrNiMo8 Steel Chain," *Metals*, vol. 7, no. 10, pp. 1-12, 2017.
- [40] P. Geng, G. Qin, J. Zhou, Z. Zou, "Hot deformation behavior and constitutive model of GH4169 superalloy for linear friction welding process," *Journal of Manufacturing Processes*, vol. 32, pp. 469-481, 2018.
- [41] R. Turner, J.C. Gebelin, R.M. Ward, R.C. Reed, "Linear friction welding of Ti-6Al-4V: Modelling and validation," *Acta Materialia*, vol. 59, no. 10, pp. 3792-3803, 2011.
- [42] P.K. Zhao, L. Fu, D.C. Zhong, "Numerical simulation of transient temperature and axial deformation during linear friction welding between TC11 and TC17 titanium alloys," *Computational Materials Science*, vol. 92, pp. 325-333, 2014.
- [43] S. Ji, Y. Wang, J. Liu, X. Meng, J. Tao, T. Zhang, "Effects of welding parameters on material flow behavior during linear friction welding of Ti6Al4V titanium alloy by numerical investigation," *International Journal of Advanced Manufacturing Technology*, vol. 82, p. 927-938, 2016.
- [44] L. Maio, F. Franco, A. Squillace, L. Lecce, "A simplified approach to numerical simulation of LFW process of Ti6Al4V alloy: investigation on friction and temperature," *International Journal of Advanced Manufacturing Technology*, vol. 86, p. 3217-3228, 2016.
- [45] M. Grujicic, R. Yavari, J.S. Snipes, S. Ramaswami, C.F. Yen, B.A. Cheeseman, "Linear Friction Welding Process Model for Carpenter Custom 465 Precipitation-Hardened Martensitic Stainless Steel," *The Journal of Materials Engineering and Performance*, vol. 23, no. 6, pp. 2182-2198, 2014.
- [46] M. Grujicic, R. Yavari, J.S. Snipes, S. Ramaswami, "A linear friction welding process model for Carpenter Custom 465 precipitation-hardened martensitic stainless steel: A weld microstructure-evolution analysis," *Proceedings of the Institution of Mechanical Engineers, Part B: Journal of Engineering Manufacture*, vol. 229, no. 11, pp. 1997-2020, 2015.
- [47] M. Grujicic, G. Arakere, B. Pandurangan, C.F. Yen, B.A. Cheeseman, "Process Modeling of Ti-6Al-4V Linear Friction Welding (LFW)," *The Journal of Materials Engineering and Performance*, vol. 21, no. 10, pp. 2011-2023, 2012.

- [48] R. Turner, R.M. Ward, R. March, R.C. Reed, "The Magnitude and Origin of Residual Stress in Ti-6Al-4V Linear Friction Welds: An Investigation by Validated Numerical Modeling," *Metallurgical and Materials Transactions B - Process metallurgy and materials processing science*, vol. 43, no. 1, pp. 186-197, 2012.
- [49] X. Song, M. Xie, F. Hofmann, T.S. Jun, T. Connolley, C. Reinhard, R.C. Atwood, L. Connor, M. Drakopoulos, S. Harding, A.M. Korsunsky, "Residual stresses in Linear Friction Welding of aluminium alloys," *Materials & Design*, vol. 50, pp. 360-369, 2013.
- [50] C. Bühr, B. Ahmad, P.A. Colegrove, A.R. McAndrew, H. Guo, X. Zhang, "Prediction of residual stress within linear friction welds using a computationally efficient modelling approach," *Materials and Design*, vol. 139, pp. 222-233, 2018.
- [51] C. Bühr, P.A. Colegrove, A.R. McAndrew, "A computationally efficient thermal modelling approach of the linear friction welding process," *Journal of Materials Processing Technology*, vol. 252, pp. 849-858, 2018.
- [52] R. Turner; F. Schroeder; R.M. Ward; J.W. Brooks, "The Importance of Materials Data and Modelling Parameters in an FE Simulation of Linear Friction Welding," *Advances in Materials Science and Engineering*, vol. 2014, no. Article ID 521937, pp. 1-8, 2014.
- [53] U. U. Ofem, P. A. Colegrove, A. Addison, M. J. Russell, "Energy and force analysis of linear friction welds in medium carbon steel," *Science and Technology of Welding and Joining*, vol. 15, no. 6, pp. 479-485, 2010.
- [54] G. Buffa, D. Campanella, M. Cammalleri, A. Ducato, A. Astarita, A. Squillace, S. Esposito, L. Fratini, "Experimental and Numerical Analysis of Microstructure Evolution during Linear Friction Welding of Ti6Al4V," *Procedia Manufacturing*, vol. 1, pp. 429-441, 2015.
- [55] P. Jedrasiak, H.R. Shercliff, "Small strain finite element modelling of friction stir spot welding of Al and Mg alloys," *Journal of Materials Processing Technology*, vol. 263, pp. 207-222, 2019.
- [56] P. Jedrasiak, H.R. Shercliff, "Finite element analysis of heat generation in dissimilar alloy ultrasonic welding," *Materials & Design*, vol. 158, pp. 184-197, 2018.
- [57] M. Fukuhara, A. Sanpei, "Elastic moduli and internal frictions of Inconel 718 and Ti-6Al-4V as a function of temperature," *Journal of Materials Science Letters*, vol. 12, no. 14, pp. 1122-1124, 1993.
- [58] P.A. Colegrove, H.R. Shercliff, R. Zettler, "Model for predicting heat generation and temperature in friction stir welding from the material properties," *Science and Technology of Welding and Joining*, vol. 12, no. 4, pp. 284-297, 2007.
- [59] P.A. Colegrove, H.R. Shercliff, "CFD modelling of friction stir welding of thick plate 7449 aluminium alloy," *Science and Technology of Welding*, vol. 11, no. 4, pp. 429-441, 2006.

List of Figures:

Figure 1 Linear friction welding: (a) initial phase, (b) transition phase, (c) equilibrium phase, (d) deceleration and forge phase (after [2]).

Figure 2 Small strain analysis of linear friction welding: (a) heat input history; (b) thermal model; (c) deformation model; (d) workpiece velocity

Figure 3 Joint dimensions (the same dimensions, in mm, for both workpieces). Thermocouple locations shown in the two sections A-A, B-B, at distances of 0, 0.5, 1.5 and 2mm from the interface.

Figure 4 Iterative axial shortening in the thermal model.

Figure 5 (a) Predicted power history inferred from the thermal model; (b) corresponding temperature histories (dashed lines) and thermocouple data (solid lines), for given (initial) distances from the interface.

Figure 6 Flow stress of Ti-6Al-4V (datapoints – experimental data, solid lines – model) [41] (The highlighted region is shown enlarged in a later material deformation map, Fig.14).

Figure 7 Axial shortening as a function of time in the small-strain LFW model.

Figure 8 LFW deformation model – geometry, mesh, loads and boundary conditions.

Figure 9 Displacement $x(t)$, defining the timescales of the deformation model: (a) selected oscillation cycles during the weld; (b) quarter-cycle of a single oscillation; (c) single snapshot model. The process for averaging the power prediction over half a cycle is shown in (d).

Figure 10 Heat generation as a function of time for a typical snapshot model, showing the transition to a constant plastic dissipation rate.

Figure 11 Predicted heat generation rate vs time from the deformation model (blue), and reverse engineered from thermocouple data using the thermal model (red).

Figure 12 Cross-section through the weld at the beginning of the equilibrium stage: (a) predicted distribution of heat generated per unit volume close to the interface; (b) corresponding equivalent plastic strain at the interface; (c) experimental weld cross-section showing weld zone (WCZ) and thermomechanically affected zone (TMAZ).

Figure 13 Mapping heat generation onto constitutive data in a material deformation map.

Figure 14 Material condition maps showing flow stress of Ti6Al4V as a function of temperature and strain rate, with the dominant conditions for heat generation in a linear friction welding at weld times of (a) 0.65s (beginning of equilibrium stage); (b) 0.85s; and (c) 1s (end of equilibrium stage).

List of Tables:

Table 1 Key modelling issues and approaches to their solution in the literature.

Table 2 Summary of timescales shown in deformation analysis.